Electronic Supplementary Material (ESI) for Journal of Materials Chemistry A.

Supporting Information

Amorphous Precursor Route to the Conformable Oriented Crystallization of $CH_3NH_3PbBr_3$ in Mesoporous Scaffolds: Toward Efficient and Thermally Stable Carbon-based Perovskite Solar Cells

*Haining Chen†, Xiaoli Zheng†, Qiang Li, Yinglong Yang, Shuang Xiao, Chen Hu, Yang Bai, Teng Zhang, Kam Sing Wong, Shihe Yang**

1. Supplementary results:

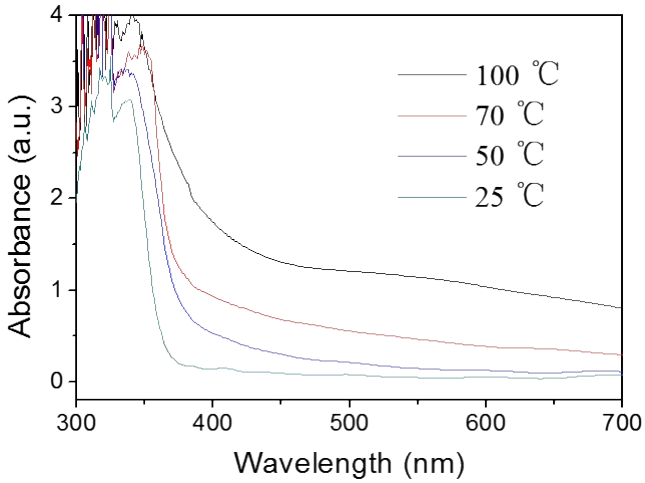

Figure S1. Uv-vis spectra of the Pb-Br precursors obtained at different temperatures. The Pb-Br precursors obtained at higher temperature exhibit higher absorption intensity, due to the more rough surface morphology.

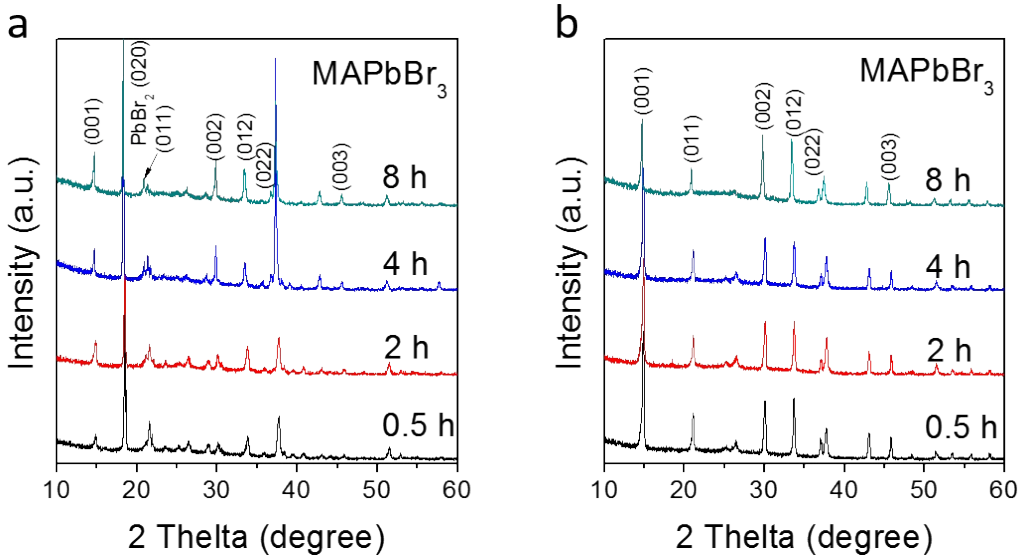

Figure S2. XRD patterns of the $MAPbBr_3$ with different reaction time in MABr IPA solution for (a) 100-Pb-Br and (b) 25-Pb-Br precursors. Relative analysis has been present in the main text.

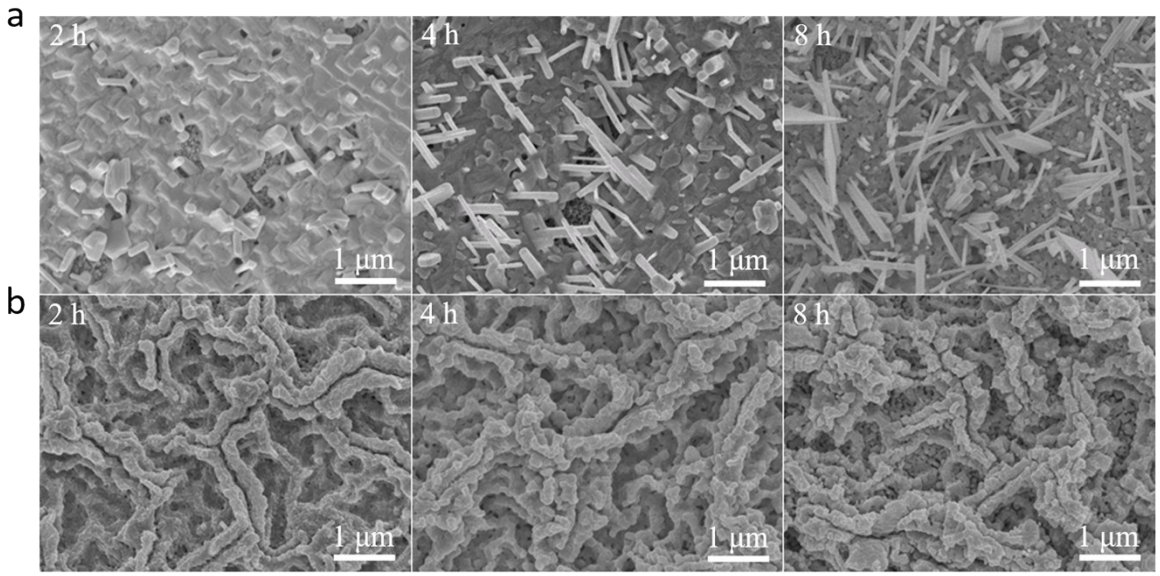

Figure S3. Change of $MAPbBr_3$ morphologies with reaction time in MABr IPA solution: (a) 100-Pb-Br and (b) 25-Pb-Br. For100-Pb-Br precursor, extending the conversion time from 2 to 8 h increases the size and density of rod-shape crystals. And the grain size of the bottom layer become smaller, partially suggesting a slight dissolving at the later conversion stage. For 25-Pb-Br precursor, the whole $MAPbBr_3$ layer tends to become smaller as conversion time increases from 2 to 8 h, also demonstrating the dissolving phenomenon. The dissolving phenomenon should be attributed to the moderately polar IPA solvent. However, no obvious large crystals are observed, indicating a neligible Ostwald ripening process for $MAPbBr_3$ system, which is different from that for $MAPbI_3$ system, as reported in our previous work.

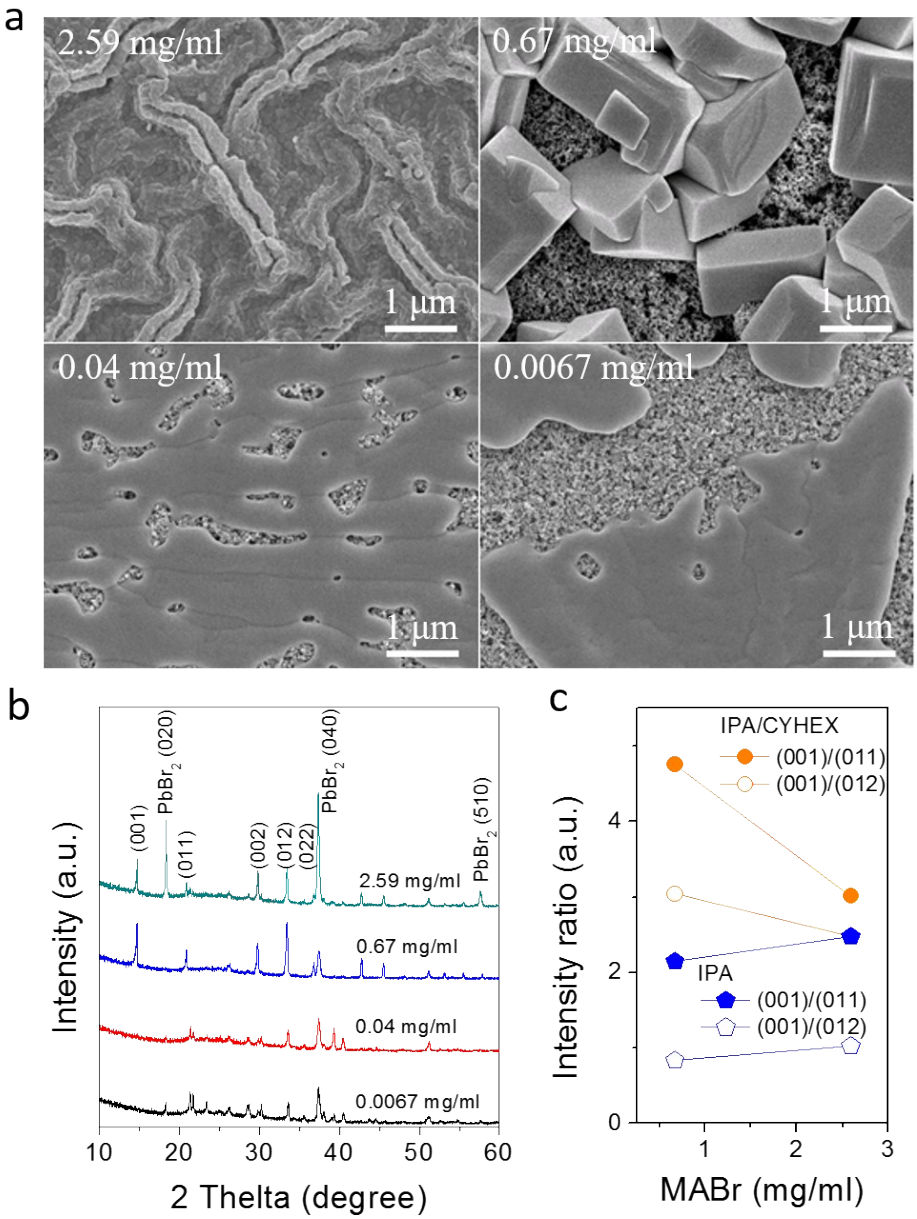

Figure S4. Morphologies and composition of the $MAPbBr_3$ obtained by changing the MABr concentrations in IPA for 25-Pb-Br precursor. (a) top-view SEM images, (b) XRD patterns and (c) relation of the intensity ratio of different planes with MABr concentrations. The concentrations of MABr in IPA are chosen according to the C_{sat} of MABr in the mixed solvent with different CYHEX concentrations, and the MABr concentrations of 2.59 mg/ml, 0.67 mg/ml, 0.04 mg/ml and 0.0067 mg/ml correspond to the C_{sat} of MABr in 50 %, 80 %, 90 % and 95 % CYHEX, respectively. As indicated, rough surface with full coverage is also observed for the $MAPbBr_3$ from 2.59 mg/ml due to the severe nucleation. But $PbBr_2$ is still present due to the retarded crystal growth. Decreasing the concentration to 0.67 mg/ml obtains obviously large crystals and the coverage becomes poor due to the localized nucleation at so low concentration, which seems to favor the conversion because of the more efficient solution penertration deep into the bottom layer through the exposed scaffold. As the concentration further decreases to 0.04 mg/ml and 0.0067 mg/ml, no conversion has happened. Since the conversion happens at 0.04 mg/ml MABr in IPA/CYHEX, it is concluded that lowering solvent polarity helps to promote the conversion process, as similar with that for $MAPbI_3$ system. Besides the higher intensity ratios of (001)/(011) and (001)/(012) at the same concentration in IPA/CYHEX suggests higher [001] orientation, which is also related to lower solvent polarity.

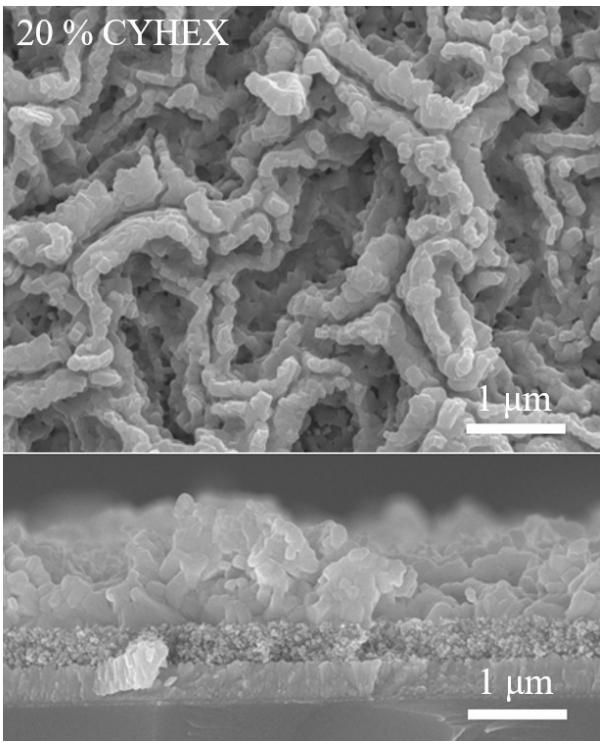

Figure 5. SEM image of the $MAPbBr_3$ obtianed from the conversion of 25-Pb-Br in the mixed solvent containing 20 % CYHEX for 30 min, which still exhibits very rough surface.

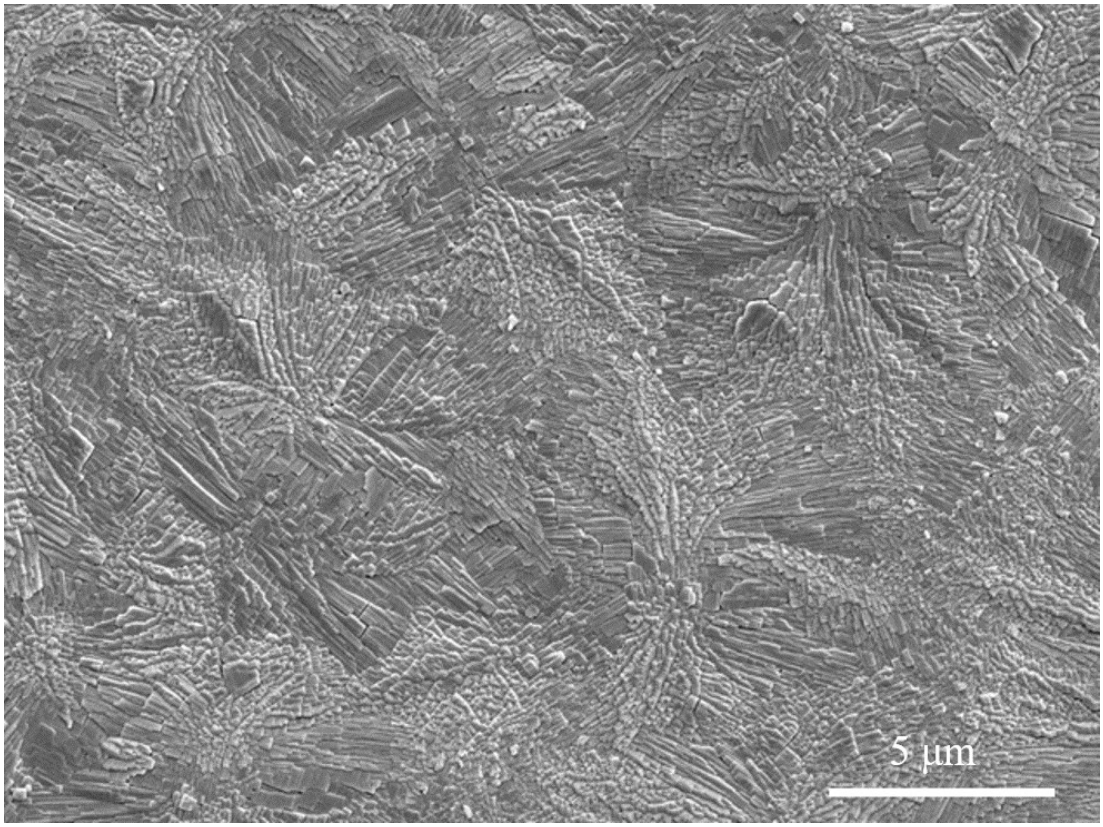

Figure S6. Low magnification SEM image of the 25-IPA/CYHEX $MAPbBr_3$ after 8 h conversion, indicating a uniform morphology.

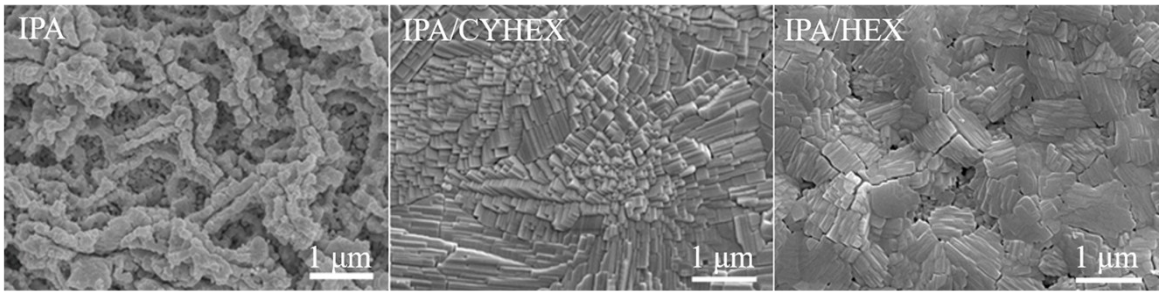

Figure S7. Top-view SEM images of the $MAPbBr_3$ films prepared from converion reactions of the 25-Pb-Br in IPA, IPA/CYHEX and IPA/HEX for 8 h. It should be noted that the SEM images for IPA and IPA/CYHEX are the same as in Figure S3b and Figure 6d. Simlar morphologies are obtained for the $MAPbBr_3$ films fabricated by converting the 25-Pb-Br in MABr IPA/HEX (1/9) and IPA/CYHEX (1/9) solution, demonstrating the generality of our method and excluding the possible peculiar effects of CYHEX.

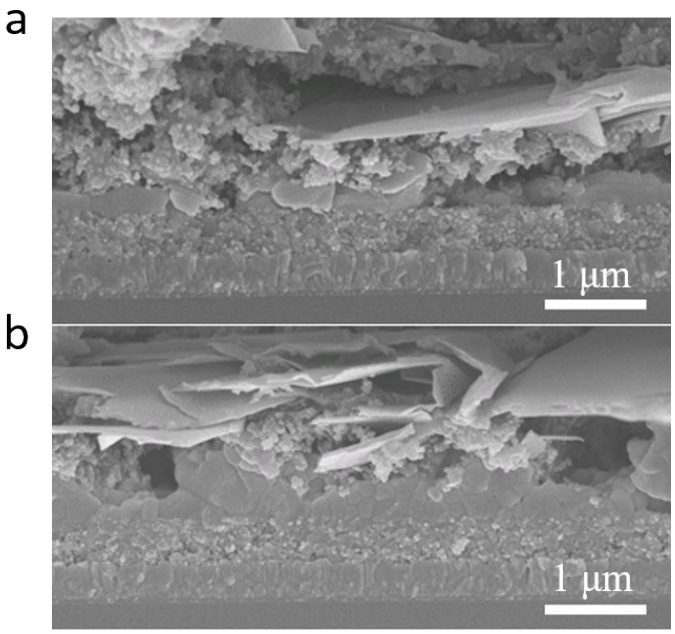

Figure S8. Cross-sectional SEM images of the carbon-based PSCs using (a) 100-IPA and (b) 25-IPA $MAPbBr_3$. As indicated, carbon electrode tends to contact with the exposed TiO_2 scaffold in 100-IPA device, while the rough $MAPbBr_3$ leads to a poor contact at $MAPbBr_3$/carbon interface in 25-IPA device.

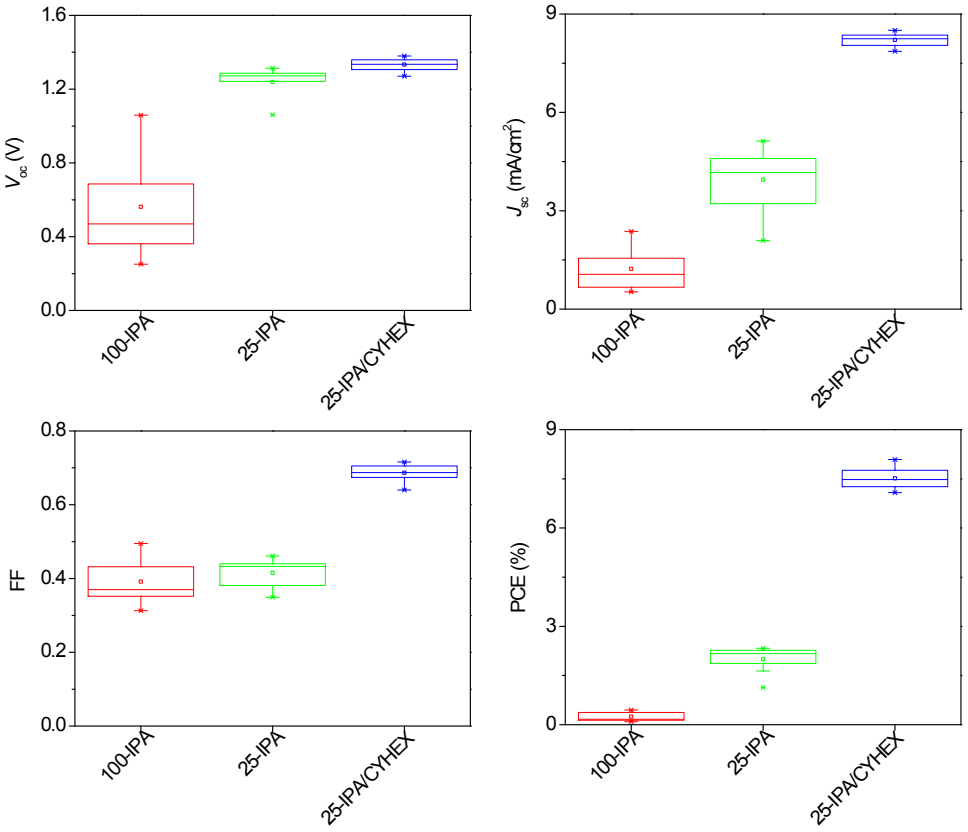

Figure S9. Photovoltaic performance distributions of the C-PSCs based on different $MAPbBr_3$ films. All the photovoltaic parameters for the 25-IPA/CYHEX device demonstrated the considerably higher reproducibility.